A VIRTUAL TUBE DELAY EFFECT

Riccardo Simionato
University of Padova
Dept. of Information Engineering
Padova, Italy
riccardo.simionato.vib@gmail.com

Juho Liski , Vesa Välimäki*
Aalto University, Acoustics Lab
Dept. of Signal Processing and Acoustics
Espoo, Finland
juho.liski@aalto.fi

Federico Avanzini
University of Milan
Dept. of Computer Science
Milan, Italy
federico.avanzini@di.unimi.it

ABSTRACT

A virtual tube delay effect based on the real-time simulation of acoustic wave propagation in a garden hose is presented. The paper describes the acoustic measurements conducted and the analysis of the sound propagation in long narrow tubes. The obtained impulse responses are used to design delay lines and digital filters, which simulate the propagation delay, losses, and reflections from the end of the tube which may be open, closed, or acoustically attenuated. A study on the reflection caused by a finite-length tube is described. The resulting system consists of a digital waveguide model and produces delay effects having a realistic low-pass filtering. A stereo delay effect plugin in PURE DATA[1] has been implemented and it is described here.

1. INTRODUCTION

Analog and digital delays are at the basis of several audio effects, including vibrato, flanger, chorus, echo, as well as spatial effects such as reverberation [1]. This paper investigates in particular the delay effects produced by a long narrow tube and presents a digital model of sound propagation in such a medium, including time delay, propagation losses, and end-reflections.

The first analog audio effect based on a narrow long tube was proposed in 1960 [2]. Olson and Bleazey presented a synthetic reverberator built with a tube, a loudspeaker, transducers, and a microphone delay unit in combination with a feedback system. A horn-loudspeaker coupled to a tube with three microphones located at different distances realized three different delays that, in conjunction with a positive feedback system, provided time spaced components.

In 1971, Bill Putman and Duane H. Cooper designed a garden-hose-based mechanical delay[2]. The echo-free acoustic delay device, called the Cooper Time Cube, sends audio through long coiled tubing with mic capsules, used as speakers and pickups, to create a time delay. In addition, a series of tooled aluminum blocks tune the delay to a relatively flat response.

Examples of simulated analog delay system are the Echoplex Tape Delay [3], and the Bucket Brigade Device [4]. The Echoplex is a tape delay device with fixed playback and erase heads, a movable record head, and a tape loop. A simulation using a circular buffer and pointers moving along it was presented in [3]. The bucket-brigade device instead realizes a time delay with an analog circuit. The input signal is sampled in time and passed into a series of capacitors and MOS transistor switches. The device is modeled with low-order digital infinite impulse-response (IIR) filters based on the resistance and capacitance values of the filters [4].

Other delay-based system examples are the spring [5, 6, 7] and plate reverbs [8, 9]. Spring reverberation is an electromechanical effect based on metal springs [10]. A first simulation by measuring the response of a real spring reverberation unit and by using digital waveguide methods was proposed in [5]. Two other methods involving a finite difference scheme [6], and by using delay-network reverberation techniques [7] were later presented. Instead, plate reverberation uses steel plates under tension [11], and it can be simulated with finite difference methods [8] and by using a hybrid structure consisting of a short convolution section and a feedback delay network [9].

The reverberation and coloration caused by a long tube has also been shown to be a robust cue for the distance perception of a sound source [12]. In a recent study, a digital-waveguide-mesh model of a small tubular shape has been used to simulate distance in a virtual environment [13]. The virtual tube delay effect presented in this paper can also be employed for this application.

Digital waveguide modeling for wave propagation in cylindrical and conical instruments is often used [14, 15, 16]. A technique for estimating a waveguide model of wind instrument from acoustic tube measurements was also presented in [17].

The rest of the paper is organized as follows. An overview of the performed measurements is given in Sec. 2, while their analysis is presented in Sec. 3. Sections 4 and 5 describe the approach used to design the digital propagation and reflections filters, which are then compared to the measurements in Sec. 6 in order to provide an objective evaluation of the results. Section 7 presents and discusses the implementation of a real-time plugin in the PURE DATA environment. Finally, Sec. 8 concludes this paper.

Supplementary materials including the plugin, the externals for MAC OS X and LINUX, the source C++ file, and some dry sounds are available for download at https://github.com/RiccardoVib/VIRTUAL_TUBE_DELAY-EFFECT-.

2. ACOUSTIC TUBE DELAY MEASUREMENT

Three different tubes were used with an internal diameter of 1.2, 1.9 and 2.5 cm, respectively. The first tube was 8.8 m long and the other ones 25 m. The tube responses were measured with a logarithmic sine sweep that was played back to the tube with a full range loudspeaker. Figure 1 shows the equipment and the setup of the measurements.

The measurements were conducted in an anechoic chamber and in two modalities: closed end and open end. The goal of the first modality was to obtain a clean impulse response caused by propagation and losses without any reflections. Polyurethane and a metal plate were used to absorb and block reflections from the

* J. Liski's work was supported by the Aalto ELEC Doctoral School.

[1] http://puredata.info.

[2] https://www.uaudio.com/blog/cooper-time-cube-power/.

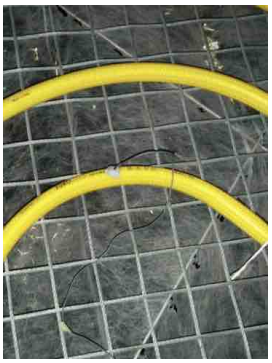

(a) Microphone inside the tube with gray moldable plastic to attach it to the hole.

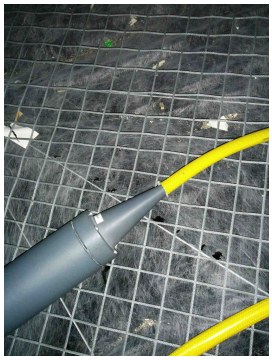

(b) Loudspeaker attached to the end of the tube with a conical adaptor.

(c) Short narrow tube (length 8.8 m, inner diameter 1.2 cm).

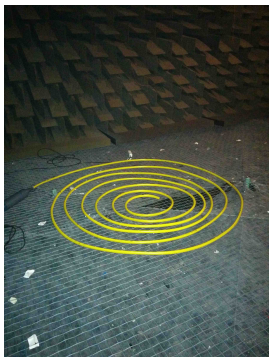

(d) Long medium-sized tube (25 m, 1.9 cm).

Figure 1: *Measurement setup in the anechoic chamber.*

tube end. The measurements with the open end were performed by using the acoustic pulse reflectometry technique [18] and required further analysis of the reflection behavior, as the impulse responses contained clearly observable repeating reflections. The polyurethane and the metal plate were chosen based on initial experiments to minimize the reflections from the end.

Ten holes were drilled 1 m apart along the length of the tube starting 2.5 cm from the loudspeaker end of the tube. Multiple measurements were made, recording the response of one hole at a time with a miniature microphone while blocking the others with moldable plastic material in order to avoid a "flute finger-hole effect" in the recordings. In addition, in order to record the cleanest possible impulse responses, the measurements were taken from hole positions drilled up to 10 m from the loudspeaker end of the tube to ensure at least 15 m of length to the opposite end (and a round-trip travel distance of 30 m before returning to the microphone). An exception was made with the 1.2 cm diameter tube, since it was only 8.8 m long.

The impulse response of the system was computed using Farina's method, convolving the recorded signal with the time-inverted logarithmic sweep [19]. The input signal was 3 s long and with an amplitude of -41 dB, chosen after several experiments in order to find a trade-off between the signal-to-noise ratio and the harmonic distortion. The average SNR in the measurements ranged from 50 dB (for the narrowest tube) up to 40 dB (in the largest one).

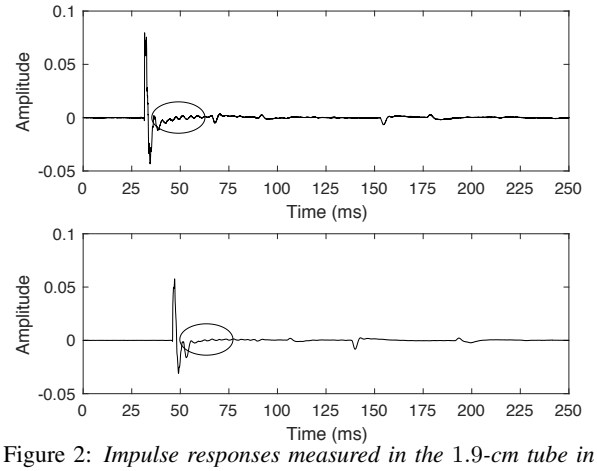

Figure 2: *Impulse responses measured in the* 1.9*-cm tube in the open end case, at the distance of* 4.25 *m (top) and* 9.25 *m (bottom).*

Finally, the measurements were performed with a sample rate of 44.1 kHz.

3. TUBE DELAY ANALYSIS

Figure 2 shows two example impulse responses collected in the open-end mode. The main spike of the impulse response followed by some ripple, identified with circles, and reflections can be seen. The ripple is due to the holes along the tube. The holes could not be filled completely, and the resulting cavities created small reflections.

Due to the finite length of the tube, the microphone recordings contain reflections from both ends. The waves propagating through the tube are reflected at the open end and, coming back, they are reflected again from the loudspeaker. Reflections appear in pairs repeated in time and progressively attenuated along the response. The location of the impulses can also be seen to differ between the two measurements in Fig. 2 due to the increased distance of the microphone from the loudspeaker.

3.1. Impulse Response Analysis

The measured responses were windowed in time to remove harmonic distortion components and unwanted reflections. A processed impulse response is presented in Fig. 3. The frequency response exhibits losses in the high end of the spectrum caused by propagation losses through the tube. There are also some losses in the low frequencies caused by the windowing. Significant attenuations of 20 dB or more appear above about 300 Hz.

As expected, spectral analysis of the windowed responses exhibits highly attenuated behavior at very high frequencies, as seen in the example in Fig. 3. This can be caused in part by the effect of non-planar wave propagation above the cutoff of planar waves. The behavior of the spectrum in the extreme high end is very noisy and, thus, unreliable.

The group delay was also computed. It showed an approximately flat response, indicating no time delay between the various sinusoidal components of the signal. This suggests that a delay line is suitable for simulating the propagation delay.

Figure 4 (left) shows the impulse responses recorded at three different holes. The time delay and the propagation loss can be

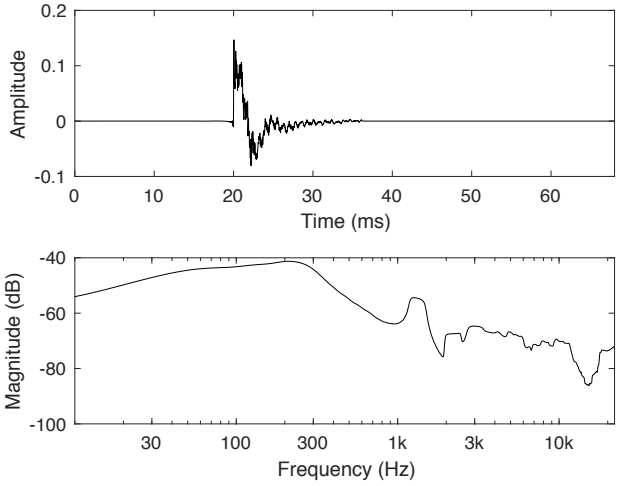

Figure 3: *Example of windowed impulse response (top) obtained from the* 2.5*-cm tube and its magnitude spectrum (bottom).*

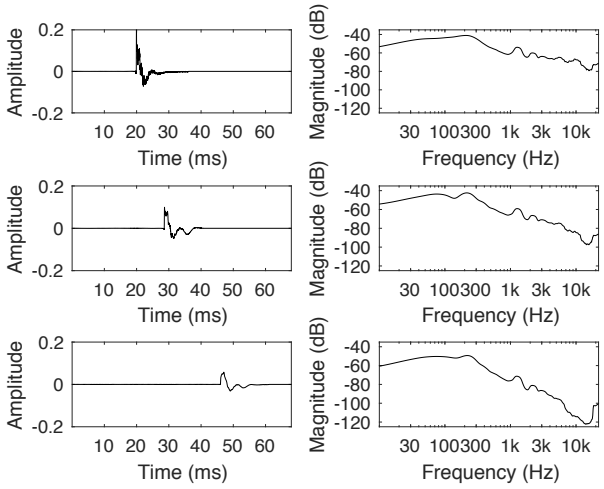

Figure 4: *Impulse response measured (left) and corresponding magnitude responses (right) in the* 1.9*-cm garden hose at the distance of* 2.5 *cm (top),* 3.25 *m (middle), and* 9.25 *m (bottom) from the loudspeaker.*

observed here. Their corresponding frequency contents are shown in Fig. 4 (right), and they reveal an increase of the attenuation with the increasing distance traveled and more significant losses at high frequencies when compared to low frequencies.

In addition, our measurements show that energy losses at high frequencies depend on the diameter of the tube. This behavior can be observed in Fig. 5, where the windowed responses captured at 4.25 m from the beginning of the tube, together with their corresponding frequency spectra, are shown for the three different tube diameters 1.2, 1.9, and 2.5 cm. The attenuation is seen to increase with decreasing diameter, showing more losses especially at high frequencies.

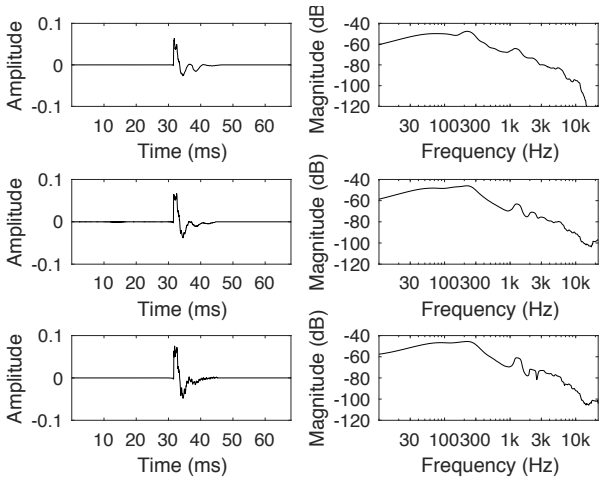

Figure 5: *Impulse response measured (left) and corresponding magnitude responses (right) at the distance of* 4.25 *m in the* 1.2*-cm (top),* 1.9*-cm (middle), and* 2.5*-cm (bottom) tube.*

3.2. Reflection Analysis

Figure 2 shows the behavior of the reflections at the closest and the farthest hole to the loudspeaker. The negative reflection and the positive one can be clearly seen. The gap between reflections depends on the position of the microphone which recorded them. The farthest hole is 9.25 m from the loudspeaker and 15.75 m from the open end, which means a longer distance for the reflections to meet the microphone.

The reflections were windowed as well. The analysis shows that energy exhibits losses in the high end of the spectrum and, instead, it is concentrated in the low frequencies. Figure 6 shows the windowed reflection result at the tube end together with its spectrum. From 300 Hz up to 1.5 kHz the spectrum exhibits a steep slope and above that extreme low energy values. The inverted pressure pulse due the open end can also be noticed.

4. VIRTUAL TUBE MODEL

The spectra of all the windowed signals were analyzed collectively. More specifically, in order to analyze the spectral changes associated with each meter traveled through the tube, the differences in the spectra of the respective signals were computed with the following equation:

$$\frac{H^i_{\text{dB}}(f) - H^j_{\text{dB}}(f)}{d_{ij}} \quad \forall i, j \,, \tag{1}$$

where $H_{\text{dB}}(f)$ is the spectrum magnitude of the signal in decibels, smoothed with a third-octave filter, and d_{ij} the distance in meters between the i-th and j-th holes, where the signals were recorded. These differences were computed for each tube. Then, the arithmetic mean of the results obtained was computed for each tube. In this way, an average behavior for a 1 m segment of each tube was obtained. The results are shown together in Fig. 7.

It can be noticed that the attenuation increases towards the high end of the spectrum and that it depends on the tube diameter.

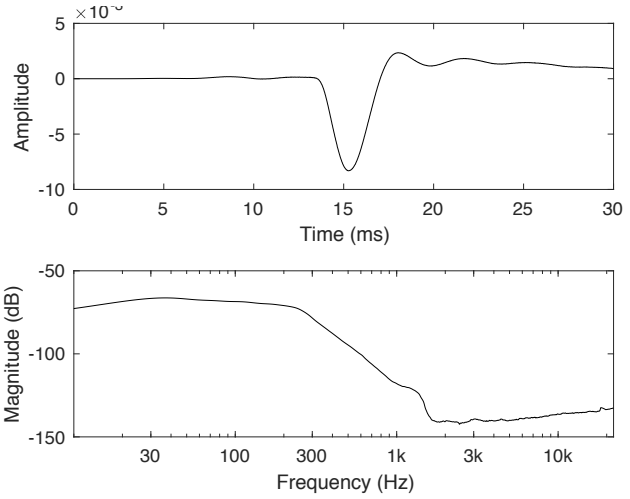

Figure 6: *A windowed reflection (top) and its magnitude spectrum (bottom) recorded with the* 1.9*-cm tube.*

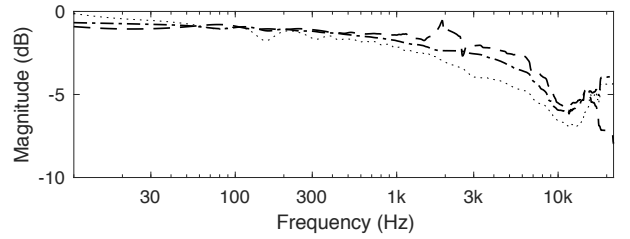

Figure 7: *Average "difference filters" for a* 1*-m segment (see Eq. (1)) of a* 1.2*-cm (dotted line), a* 1.9*-cm (dash-dot line), and a* 2.5*-cm (dashed line) tube.*

Increasing diameters result in a steeper shape, but with smaller attenuation. The responses below 300 Hz, despite some oscillations, are very similar to each other near 0 dB. Attenuation is noticeable above 300 Hz and becomes more significant around 1 kHz.

Since the first modes of the tubes are at 8054 Hz, 10598, and 16780, the results above these frequencies are unreliable. For this reason, the responses above these frequencies were not considered, and a continuous slope for the frequencies larger than 10 kHz in the design of the filters was taken.

Based on the above considerations, the spectrum can be assumed to have a low-pass shape. Increasing the tube diameter decreases the spectral slope and increases the cutoff frequency.

4.1. Reflections from the End of the Tube

In order to understand the effect of the open end on the responses, a different approach was chosen. Using the acquired information, the impulse response measured at the farthest hole from the loudspeaker was filtered with the filter approximating an appropriate power of the 1 m segment shape of Fig. 7. The filter design procedure will be described in Sec. 5. The aim here was to simulate the losses of the same distance that the reflected pulse had traveled. This simulation could be compared with the reflection, separating the reflection effect of the open end. The distance traveled by

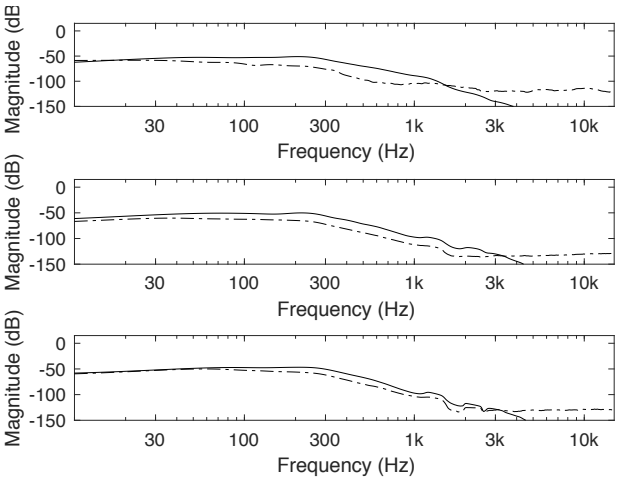

Figure 8: *Comparison between the spectrum of the reflection captured by the microphone (dash-dot line), and the simulated spectrum as it should be without the open end effect (solid line):* 1.2*-cm (top) ,* 1.9*-cm (middle) and* 2.5*-cm (bottom) diameter tubes.*

the reflection was computed and used to build the filter, accounting for the approximation error which becomes significant for long distances.

Figure 8 shows the spectrum of the reflection captured by the microphone and the simulated spectrum as it should be without the open-end effect. A slight attenuation can be seen below 100 Hz, and a stronger one up to 1 kHz. Since the impulse travels along the whole tube before reaching the open end, it has very low energy above 3 kHz and the recorded reflection is superimposed by the noise. When the impulse crosses the boundary at open end, the pressure wave hits the outside air, at atmospheric pressure, creating a compression wave heading back down the tube with some energy left.

Using the filter designed for the tube model, the effect of the reflection R due the open end was obtained:

$$R = \frac{H^i_{\text{ref}}(f)}{H^i_{\text{sim}}(f)}, \tag{2}$$

where $H_{\text{sim}}(f)$ is the spectrum of the response without the open end effect simulated with the approach described above using the same distance traveled by the corresponding windowed reflection $H_{\text{ref}}(f)$. This allows for the estimation of how the reflection affects the spectrum. Equation (2) was estimated for each measure where the reflections were isolated enough and could be windowed. Finally, the average for each tube size was computed. The shapes shown in Fig. 9 summarize the results.

The results show that the attenuation depends on the diameter of the tube, starting with a low value increasing above 100 Hz. The attenuation becomes smaller at higher frequencies because of the noise level.

5. FILTER DESIGN

This section describes the design of the filters simulating the sound propagation through the tube and the reflection effect by the open

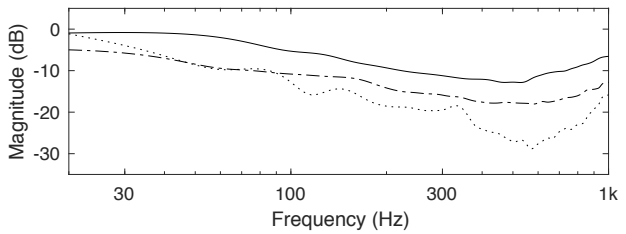

Figure 9: *Average filters estimating the open end effect (see Eq. (2)) of a* 1.2*-cm (dotted line),* 1.9*-cm (dash-dot line), and* 2.5*-cm (dashed line) tube.*

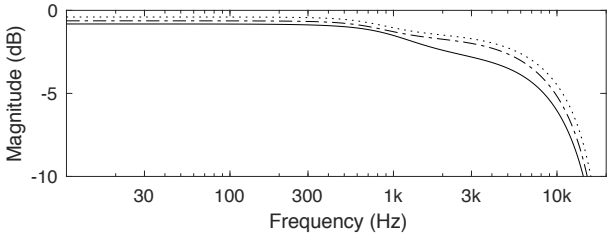

Figure 10: *Low-order approximations of the average "difference filters" for a* 1*-m segment (see Eq. (1)):* 1.2*-cm (solid line),* 1.9*-cm (dash-dot line), and* 2.5*-cm (dotted line) diameter tubes.*

end. For each of these effects, the average filters previously computed and summarized in Figs. 7 and 9 were used as target shapes to be approximated with low-order filters. Then, a unique form to interpolate between the different diameters values was found.

5.1. Propagation Filter

Given the simple shapes of these filters (see Fig. 7), attempts were made to find a low-order filter simulating their behavior. Keeping the three averages as targets, three parametric filters were computed, approximating the shape in order to minimize audible errors.

A cascade of two high-shelving filters and one low-pass filter was built, resulting in a 5^{th}-order parametric filter. The high-shelving filters were used to approximate the shape from 300 Hz to 3 kHz, while the low-pass filter was needed to cut the high end of the spectrum.

Since the three target shapes behave very similarly at low frequencies, the filters have the same behavior until 300 Hz with a slight attenuation depending on the diameter of the tube. The significant variations are in the range above 1 kHz, where different attenuations and cut-offs can be seen. The cut-off frequencies for the three target shapes are 4062, 5950, and 7015 Hz, respectively.

Figure 10 shows the different filters designed for the three diameter tubes to be compared with those in Fig. 7. With these low-order filters, a tube with arbitrary length can be simulated. Moreover, interpolating between the three filters allows to simulate different diameters sizes.

Since a cascade is an inefficient approach to produce tubes longer than 1 m, an approximation was found. Starting from the filter computed for the 1.2 cm tube, all the parameters of the three basic filters composing it were gradually varied in a linear way to achieve an approximated filter for longer lengths. A cascade of two 1^{st}-order low-pass filter replaced the simple 1^{st}-order one, resulting in a 6^{th}-order parametric filter. A good approximation up to 30 m (which is sufficient for the purpose of the audio effect) was obtained with an error smaller than 0.6 dB. In addition, with this method a better accuracy creating the tube can be achieved. Instead of 1 m as the incremental step, a finer control, like 1 cm, can be implemented. Figure 11 shows the approximation for 30 m. The designed filter follows accurately the general shape except for a critical range between 300 Hz and 1 kHz. In the case of 30 m tube, the maximum error is 0.57 dB.

After obtaining an accurate approximation of frequency attenuations due to propagation in the tube, the final filter was obtained by using a delay line that simulates the propagation delay and is

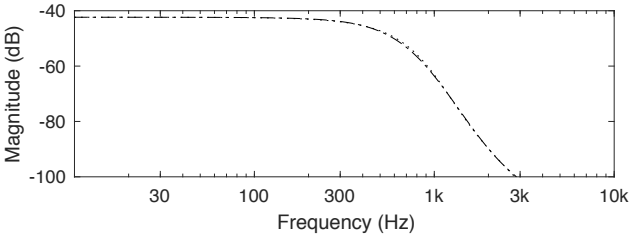

Figure 11: *Example of a parametric filter designed to approximate* 30 *m long tube: target filter (dotted line), and approximation (dash-dot line).*

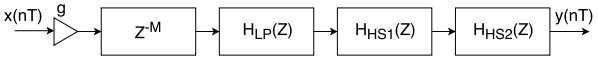

Figure 12: *Modeling the sound propagation using a delay line and three filters.*

connected in series with the previously discussed filter.

Figure 12 shows the three parametric filters in cascade and the delay line composing the system. The system can be described mathematically as follows:

$$H_{\text{tube}}(z) = g z^{-M} H_{\text{HS1}}(z) H_{\text{HS2}}(z) H_{\text{LP}}(z), \tag{3}$$

where g is a gain factor, z^{-M} is the delay line of M samples, $H_{\text{HS1}}(z)$ and $H_{\text{HS2}}(z)$ are 2^{nd}-order IIR high-shelving filters, and $H_{\text{LP}}(z)$ is a 1^{st}-order IIR low-pass filter.

The coefficients of the high-shelving and low-pass filters were computed with the usual formulas of the 1^{st}- and 2^{nd}-order filters [20]. Three different IIR filters were designed, one for each tube diameter (1.2, 1.9, 2.5 cm), giving the possibility to approximate the different behaviors by controlling the shape with the cut-off frequencies of the designed IIR digital filter.

In order to control the filter behavior as a function of the diameter of the simulated tube, the cut-off frequencies of all the filters and the gain factor g are linearly varied while the gains (dB) and the quality factors of the two high-shelving filters are kept fixed. Table 1 reports these latter values while Table 2 summarizes the filter cut-off frequencies and the gain factor for each tube diameter. Starting from these values, an interpolation was made with a granularity of 1 mm.

Table 1: *Propagation filter: gain and quality factor values for the two high-shelving filters.*

Type of filter	$G[dB]$	Q
HS1	-1	0.65
HS2	-0.9	0.5

Table 2: *Propagation filter: cut-off frequencies of low-pass and high-shelving filters and overall gain for the three tube diameters.*

Type of filter	f_{HS1} [Hz]	f_{HS2} [Hz]	f_{LP} [Hz]	g
1.2 cm	1200	1500	9500	0.85
1.9 cm	900	7000	10200	0.87
2.5 cm	900	7000	11000	0.90

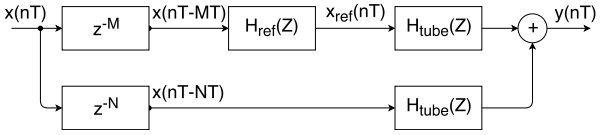

Figure 13: *Block diagram of the reflection simulation.*

5.2. Reflections

The block scheme in Fig. 13 shows the approach used to simulate the reflection. The delayed input is first filtered with the filter $H_{\text{ref}}(z)$ that approximates the losses given by the open end reflection, and the output is fed to the filter $H_{\text{tube}}(z)$ that simulates the losses caused by sound propagation in the tube. The computed reflection is finally added to the delayed sound resulting from unperturbed propagation in the tube.

The measured reflections have extremely low values in the high end of the spectrum (above 3 kHz) because of the long distance traveled. The simulation produces lower values in the high frequency region than the measured values. The extremely low values superimposed by noise produce unreliable results in this region of the spectrum. Since a steeper shape in the high frequency side due to high frequencies losses were expected, an approximation of the differences found with a continuous slope was done.

In order to approximate $H_{\text{ref}}(z)$, a cascade of a 2^{nd}-order high-shelving filter and a 1^{st}-order low-pass was chosen. Similarly to the propagation filter, by controlling the quality factors, the gains, and the cut-off frequencies, we were able to perform a linear interpolation between different diameters. An additional gain factor g_{ref} was introduced to control the scale for the different sizes. Table 3 summarizes the parameters values of the different filters.

6. COMPARISON

In this section, a comparison between the designed filters and the measurements is performed. The accuracy of the design is discussed, presenting the maximum approximation error in the frequency range of interest. Considering that the frequencies above 10 kHz are unreliable, as discussed in Sec. 4, the comparison refers the range between 20 Hz and 10 kHz.

Table 3: *Reflection filter: parameters of the low-pass and high-shelving filter and overall gain for the three tube diameters.*

Type of filter	1.2 cm	1.9 cm	2.5 cm
f_{LP} [Hz]	100	250	600
f_{HS} [Hz]	500	225	160
G_{HS} [dB]	-14	-14	-10
Q_{HS}	0.35	0.4	0.60
g_{ref}	0.4225	0.5180	0.9

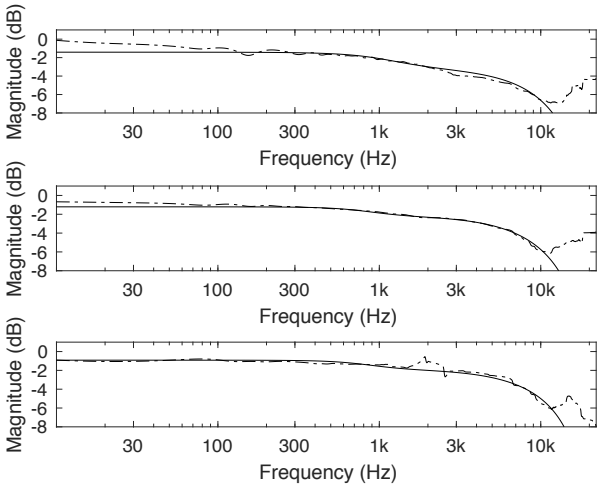

Figure 14: *Filters designed (solid line) and their corresponding targets (dash-dot line) for the* 1.2*-cm (top),* 1.9*-cm (middle) and* 2.5*-cm (bottom) tube.*

6.1. Propagation Filter

Figure 14 shows the three designed propagation filters compared with the results obtained from the measurements. The filter approximating the 1.2-cm tube has a maximum error of 0.97 dB, which is mainly due to the shelf filter having a flat magnitude response at low frequencies instead of the declining slope of the measured response as shown in the top of Fig. 14. This way, a good approximation at high frequencies is obtained, which is considered to be more important that the response below 100 Hz.

The 1.9-cm filter presents a maximum error of 0.5 dB in the lowest part of the frequency range. The fit becomes very accurate at higher frequencies as seen in Fig. 14 (middle). The error is 0.31 dB at 60 Hz and decreases close to zero at frequencies above 100 Hz.

The third filter is shown in Fig. 14 (bottom) that, with the exception of an anomaly at about 1900 Hz, also fits the target shape with good accuracy. It has a maximum error of 0.5 dB at 6184 Hz, and an error smaller than 0.3 dB in the rest of the frequency range.

6.2. Reflection Filter

Figure 15 shows the difference between the three designed reflection filters and the simulation results. In this case, the range between 20 and 500 Hz is significant for the comparison as discussed in Sec. 4.1.

The filter for the 1.2-cm diameter tube, shown in the top of

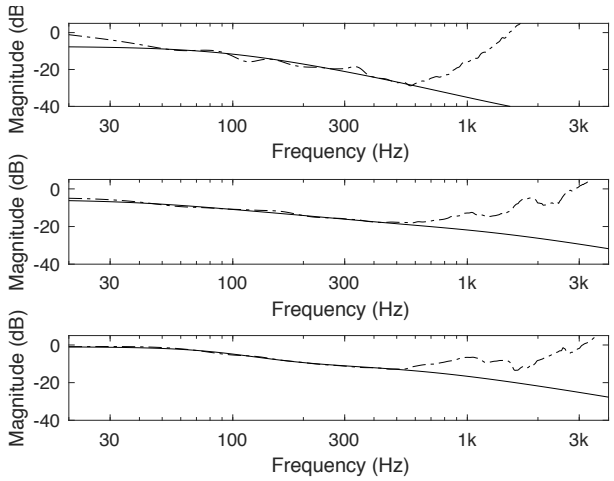

Figure 15: *Filters designed for the reflection (solid line) and their corresponding targets (dash-dot line) of the* 1.2*-cm (top),* 1.9*-cm (middle) and* 2.5*-cm (bottom) size tube.*

Fig. 14, presents the same initial behavior of the one compared in the previous section. Because of the high variability in the magnitude target, it is difficult to approximate accurately the shape, and the maximum error is 4.57 dB. The error becomes smaller than 1 dB after 60 Hz except for a deviation at 330 Hz where the error is 3.57 dB. Also in this design, a better approximation for frequencies higher than 60 Hz at the expense of the frequencies below was done.

The reflection filter for the 1.9-cm tube can be seen in the middle of Fig. 15. In the beginning of the spectrum, it has a maximum error of 1.26 dB. The error becomes smaller than 1.2 dB above 30 Hz, thus providing a good fit in the remaining range.

The third filter, as seen in Fig. 15 (bottom), is the most accurate with a maximum error of 0.52 dB at 40 Hz and close to zero above 100 Hz.

7. IMPLEMENTATION

The implementation was written in C++ as an external library for PURE DATA, an open-source real-time environment for audio processing. The stereo plugin, working at sample rate 44.1 kHz, simulates the wave propagation in a narrow tube and produces associated audio effects. It creates two virtual tubes, one for each channel. The diameter of the two tubes is always the same. The length of each tube can be set by the user and determines the desired delay in milliseconds. The speed of sound is assumed to be 345 m/s corresponding to a temperature of 23°C.

In addition, it is possible to control the volume of the delayed sound and the ratio of the dry and the wet signals in the output. The filter simulates the tube length for each 1 cm added. However, the size parameter gives the possibility to change the virtual tube diameter with a granularity of 1 mm by changing the filter parameters.

To enrich the system, the possibility of summing a reflection in the output was also implemented. This option simulates the wave reflection due the open end of the tube. A reflection, whose frequency content depends on the distance chosen for the "virtual open end," can be created for each virtual tube. This way, the length of the virtual tube becomes the sum of the length chosen for the delay effect and the length chosen in the reflection options. The sound is captured at a virtual microphone at the distance selected by combining the delayed part of the sound and the reflection coming from the end of the tube. Since the reflection captured this way is too soft to be clearly audible, a gain control was added.

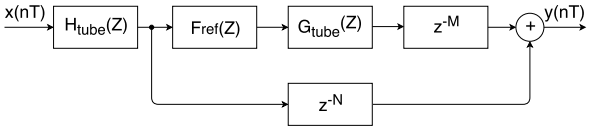

Figure 16: *Block scheme for the audio flow in the plugin.*

Including the reflection option, the system computes three filters: the filter simulating the length desired for the main delay, the filter simulating the open end, and the one simulating the residual length traveled by the sound to reach the end of the tube and come back to meet the virtual microphone. The block scheme shown in Fig. 16 summarizes the system. The residual length is represented by $G_{\text{tube}}(z)$ and is twice the length chosen in the reflection options. In order to decrease the complexity of the computation, the different coefficients of the reflection filters were pre-computed and stored.

The plugin offers the possibility to create virtual tubes up to 30 m long in default mode, and 40 m long tubes in the reflection mode. These maximums correspond to a delay of 87 ms and a reflection coming after 29 ms. Figure 17 shows a screenshot of the plugin implemented in PURE DATA.

8. CONCLUSION

A simulation of a tube delay effect was proposed in this paper. Acoustic wave propagation in garden hoses of three different diameter was measured and analyzed. Studying and elaborating the recorded tube responses, a virtual tube model was developed and a digital IIR filter controlling the length and the diameter of the virtual tube was designed with a negligible error. From the analysis of the measurements, a parametric filter was designed in which the tube diameter and length can be continuously varied. Because of the simplicity of the magnitude response shapes, a cascade of two high shelving filters and a low-pass filter was sufficient for approximating the behavior correctly. In addition, an analysis on the reflection due to the open end of the tube was conducted, and a filter approximating it was added in the model. Finally, a stereo delay effect plugin in PURE DATA was presented describing the design specifications.

9. ACKNOWLEDGMENT

This research work was conducted between August 2017 and January 2018, when Riccardo Simionato was visiting the Aalto Acoustics Lab within the framework of the Erasmus+ program.

10. REFERENCES

[1] U. Zölzer, Ed., *DAFX – Digital Audio Effects*, John Wiley & Sons, 2. edition, 2011.

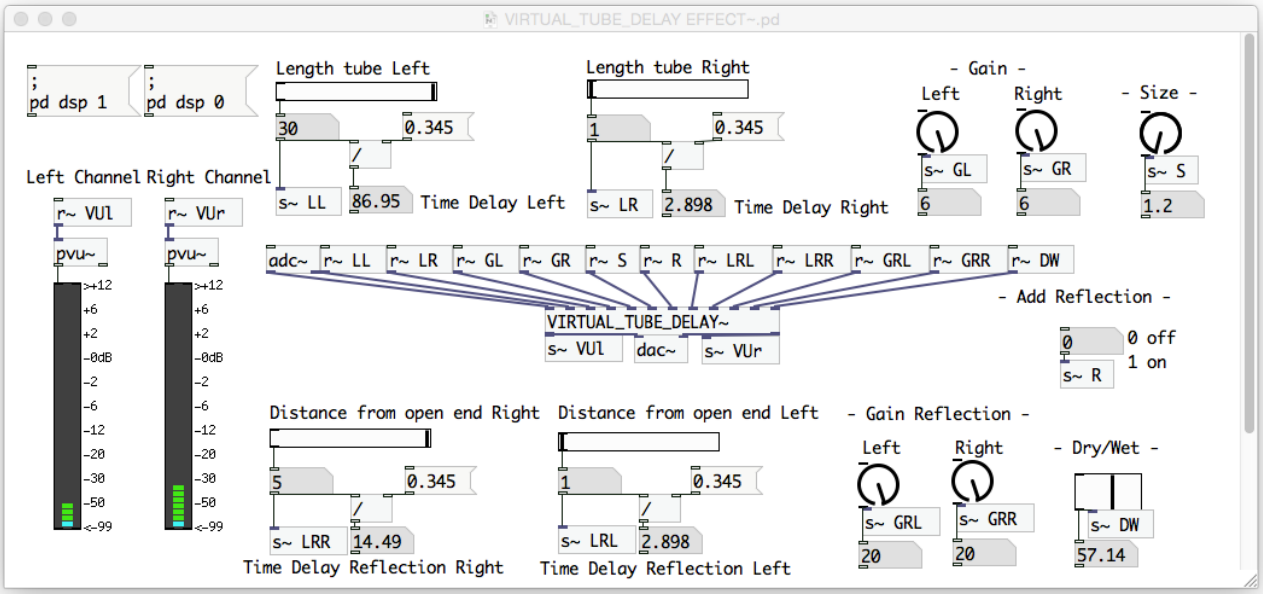

Figure 17: *The virtual tube delay effect plugin in* PURE DATA.

[2] H. F. Olson and J. C. Bleazey, "Synthetic reverberator," *J. Audio Eng. Soc.*, vol. 8, no. 1, pp. 37–41, Jan. 1960.

[3] S. Arnardottir, J. S. Abel, and J. O. Smith, "A digital model of the Echoplex tape delay," in *Proc. Audio Eng. Soc. 125th Conv.*, San Francisco, CA, USA, Oct. 2008.

[4] C. Raffel and J. Smith, "Practical modeling of bucket-brigade device circuits," in *Proc. 13th Int. Conf. Digital Audio Effects (DAFx'10)*, Graz, Austria, Sept. 2010.

[5] J. S. Abel, D. P. Berners, S. Costello, and J. O. Smith III, "Spring reverb emulation using dispersive allpass filters in a waveguide structure," in *Proc. Audio Eng. Soc. 121st Conv.*, San Francisco, CA, USA, Oct. 2006.

[6] S. Bilbao and J. Parker, "A virtual model of spring reverberation," *IEEE Audio, Speech, Language Process.*, vol. 18, no. 4, pp. 799–808, May 2010.

[7] V. Välimäki, J. Parker, and J. S. Abel, "Parametric spring reverberation effect," *J. Audio Eng. Soc.*, vol. 58, no. 7/8, pp. 547–562, Jul./Aug. 2010.

[8] S. Bilbao, "A digital plate reverberation algorithm," *J. Audio Eng. Soc.*, vol. 55, no. 3, pp. 135–144, Mar. 2007.

[9] J. S. Abel, D. P. Berners, and A. Greenblatt, "An emulation of the EMT 140 plate reverberator using a hybrid reverberator structure," in *Proc. Audio Eng. Soc. 127th Conv.*, New York, USA, Oct. 2009.

[10] J. Parker and S. Bilbao, "Spring reverberation: A physical perspective," in *Proc. 12th Int. Conf. Digital Audio Effects (DAFx'09)*, Sep. 2009, pp. 416–421.

[11] K. Arcas, "Physical modelling and measurements of plate reverberation," in *Proc. ICA*, Madrid, Spain, Sep. 2009.

[12] F. Fontana and D. Rocchesso, "Auditory distance perception in an acoustic pipe," *ACM Trans. Appl. Percpt.*, vol. 5, no. 3, 2008, Article 16.

[13] M. Geronazzo, F. Avanzini, and F. Fontana, "Auditory navigation with a tubular acoustic model for interactive distance cues and personalized head-related transfer functions," *J. Multimodal User Interfaces*, vol. 10, no. 3, pp. 273–284, Sep. 2016.

[14] V. Välimäki, *Discrete-Time Modeling of Acoustic Tubes using Fractional Delay Filters*, Ph.D. thesis, Helsinki University of Technology, Espoo, Finland, 1995.

[15] D. P. Berners, *Acoustics and Signal Processing Techniques for Physical Modeling of Brass Instruments*, Ph.D. thesis, Stanford University, Stanford, CA, USA, 1999.

[16] J. O. Smith, "Principles of digital waveguide models of musical instruments," in *Applications of Digital Signal Processing to Audio and Acoustics*, Kahrs M. and Brandenburg K., Eds., pp. 417–466. Springer, 2002.

[17] T. Smyth and J. Abel, "Estimating waveguide model elements from acoustic tube measurements," *Acta Acustica united with Acustica*, vol. 95, no. 6, pp. 1093–1103, 2009.

[18] D. B. Sharp, *Acoustic Pulse Reflectometry for the Measurement of Musical Wind Instruments*, Ph.D. thesis, The University of Edinburgh, Edinburgh, UK, 1996.

[19] A. Farina, "Simultaneous measurement of impulse response and distortion with a swept-sine technique," in *Proc. Audio Eng. Soc. 108th Conv.*, Paris, France, Feb. 2000.

[20] P. Dutilleux, M. Holters, S. Disch, and U. Zölzer, "Filters and delays," in *DAFX: Digital Audio Effects, Second Edition*, U. Zölzer, Ed., pp. 47–81. Wiley, 2011.

[21] V. Välimäki, S. Bilbao, J. Smith, J. Abel, J. Pakarinen, and D. Berners, "Virtual analog effects," in *DAFX: Digital Audio Effects, Second Edition*, U. Zölzer, Ed., pp. 473–522. Wiley, 2011.